Effective Resistivity for Magnetohydrodynamic Simulation of Collisionless Magnetic Reconnection

H W Zhang [1,2,*], Z W Ma [2], T Chen [2], X M Yu [3], C J Xiao [3]

1 Max Planck Institute for Plasma Physics, Garching, Germany

2 Institute for Fusion Theory and Simulation, School of Physics, Zhejiang University, Hangzhou, China

3 School of Physics, Peking University, Beijing, China

*Email: haowei.zhang@ipp.mpg.de

The 16th International West Lake Symposium on the "Physics of Fusion and Space Plasmas"
Hangzhou, China, April 10-12, 2026

Outline

- ❑ Introduction
- ❑ Physical model
- ❑ Verification by PIC simulation
- ❑ Validation by in-situ satellite observation and experimental data
- ❑ Application in Hall MHD simulation
- ❑ Summary and future possible applications

Outline

- Introduction
- Physical model
- Verification by PIC simulation
- Validation by in-situ satellite observation and experimental data
- Application in Hall MHD simulation
- Summary and future possible applications

Magnetic reconnection

Magnetic reconnection plays a crucial role in dynamic processes occurred in **space and laboratory plasmas**.

Earth's magnetotail

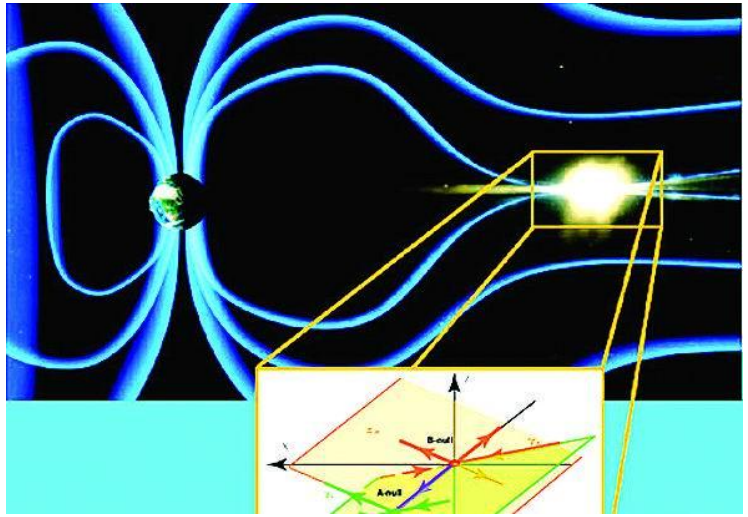

Solar corona

Magnetic reconnection

Magnetic reconnection plays a crucial role in dynamic processes occurred in **space and laboratory plasmas**.

Sawtooth / tearing mode in tokamak

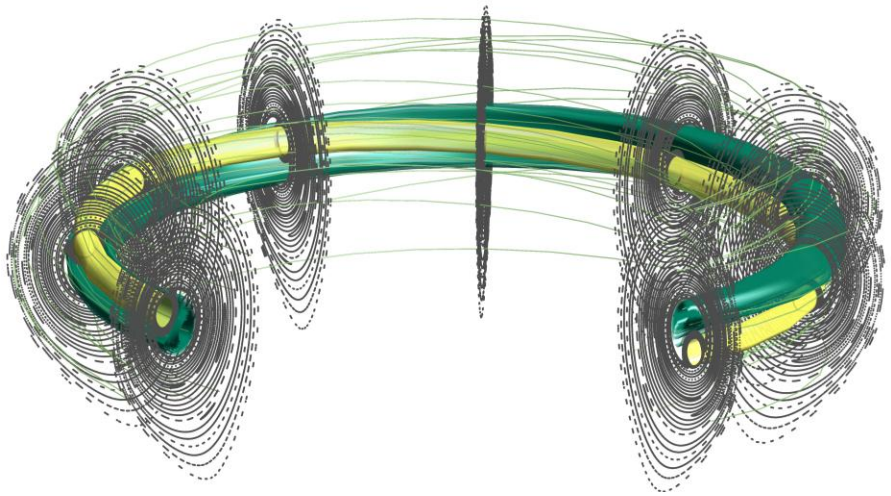

H. Zhang, et al. arXiv:2602.15431 (2026)

Helicity state in Reversed Field Pinch (RFP)

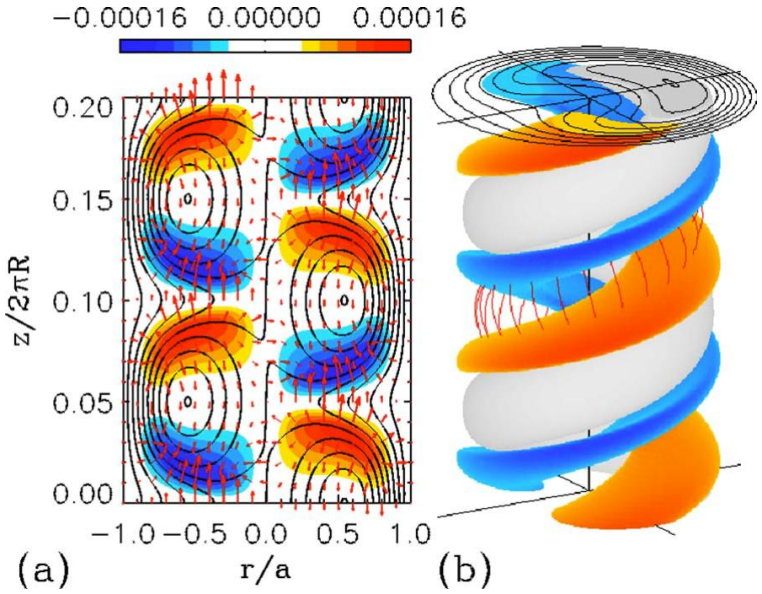

S. Cappello, et al. Phys. Plasmas 13, 056102 (2006)

Magnetic reconnection

- The **topology** of magnetic field is changed.
- Time scale must be much **faster than diffusion time scale**.
- **Magnetic energy converts into kinetic or thermal energy**, and mass, momentum, and energy transfer between two sides of the central current sheet.

However, in collisionless plasma, the Spitzer resistivity based upon electron-ion collision is too small to explain the fast magnetic reconnection ($\gamma \sim 0.1 B_0 v_A$)**.**

L. Comisso, et al. J. Plasma Phys. 82, 595820601 (2016)
Q. Lu, et al. Presentation in this meeting (2026)

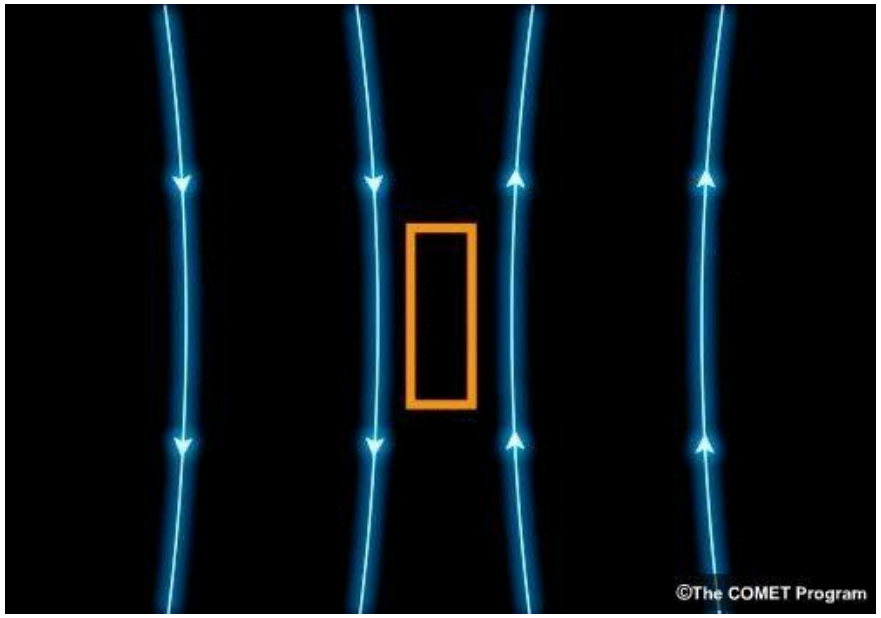

Previous explanation for reconnection electric field: the electron off-diagonal pressure term

- The momentum equation for ions and electrons in a collisionless plasma can be written as

$$m^\alpha n^\alpha \left(\frac{\partial}{\partial t} + \vec{v}^\alpha \cdot \nabla\right)\vec{v}^\alpha + \nabla \cdot \mathbf{P}^\alpha = q^\alpha n^\alpha \left(\vec{E} + \vec{v}^\alpha \times \vec{B}\right)$$

- Under the assumption of a two-dimensional process, the electron momentum equation (**generalized Ohm's law**) is

$$E_z = -\frac{m^e}{e}\left(\frac{\partial}{\partial t} + \vec{v}^\alpha \cdot \nabla\right)v_z^\alpha - \frac{1}{n^e e}\left(\frac{\partial P_{xz}^e}{\partial x} + \frac{\partial P_{yz}^e}{\partial y}\right) - \left(\vec{v}^e \times \vec{B}\right)_z$$

- It is further assumed that the v_x^e and v_y^e are relatively small near the neutral line and ignore the Lorentz force

$$E_z \simeq -\frac{1}{n^e e}\left(\frac{\partial P_{xz}^e}{\partial x} + \frac{\partial P_{yz}^e}{\partial y}\right)$$

electron off-diagonal pressure term

H. J. Cai, et al. Phys. Plasmas 4, 509 (1997)

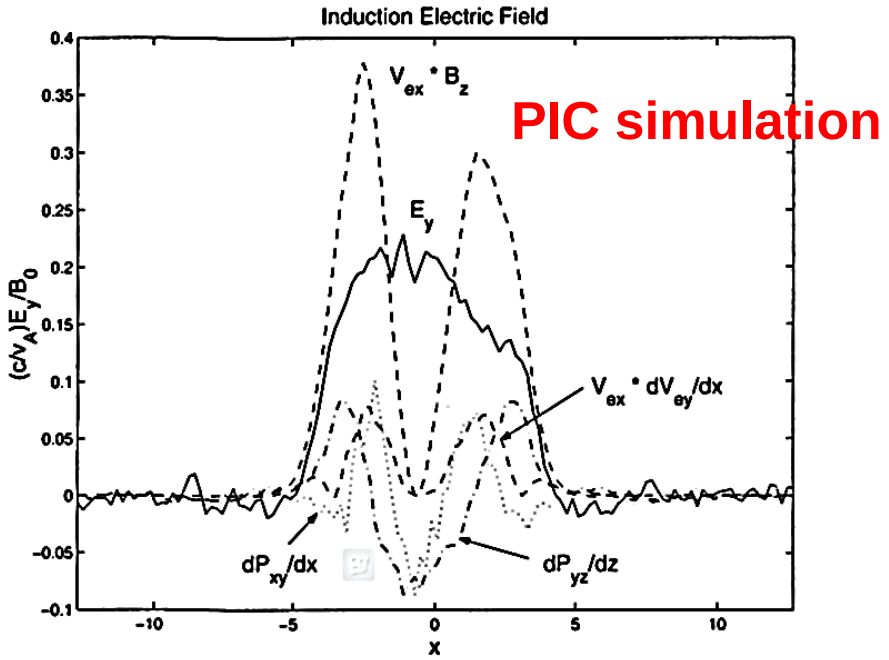

PIC simulation

Figure 5. Profile of the inductive electric field E_y averaged over the interval from $\Omega_i t = 15.0$ to 15.6 as a function of x at $z = 0$ (solid line). The additional curves represent the contributions to E_y of individual terms in (11).

P. L. Pritchett, et al. J. Geophys. Res. 106, 4783 (2001)
M. A. Shay, et al. Phys. Rev. Lett. 99, 155002 (2007)

similar results from hybrid simulation:

M. M. Kuznetsova, et al. J. Geophys. Res. 106, 3799 (2001)

Other models of effective resistivity & fast reconnection

Kinetic & Inertial Effects

- **Inertia & Gyromotion:** Conductivity determined by particle lifetime in the diffusion region and the gyro-period outside. *(T. Speiser, 1970)*
- **Electron Inertia:** The role of particle mass in reconnection dynamics. *(Andrés et al., 2014)*
- **Thermal-Inertial Effects:** Combining temperature and mass effects. *(Comisso & Asenjo, 2014)*

Current & Velocity-Driven Models

- **Drift Velocity:** Resistivity as a function of relative electron-ion drift. *(Ugai, 1995; Yokoyama & Shibata, 1994)*
- **Plasma Current:** Effective resistivity models scaling with local current density. *(Otto, 2001)*

Stochastic & Turbulent Processes

- **Chaos-Induced:** Effective resistivity emerging from chaotic particle orbits. *(Numata & Yoshida, 2002)*
- **Turbulence-Induced:** Energy dissipation driven by turbulent fluctuations. *(Eyink et al., 2013)*

Simulation & Specialized Plasmas

- **Localized resistivity:** Prescribed resistivity for Magnetohydrodynamic simulations. *(P. F. Chen et al., 1999; B. Kliem et al., 2000; Pérez-Coll Jiménez et al., 2022)*
- **Kinetic-Motivated (Pair Plasma):** Physics-informed models for electron-positron plasmas. *(Bugli et al., 2025; Selvi et al., 2023; Moran et al., 2025)*

...

Outline

- Introduction
- Physical model
- Verification by PIC simulation
- Validation by in-situ satellite observation and experimental data
- Application in Hall MHD simulation
- Summary and future possible applications

Physical Model

Classical (Spitzer) resistivity

$$\eta_{spz} = \frac{m_e \nu_{ei}}{e^2 n_e}$$

Coulomb collision

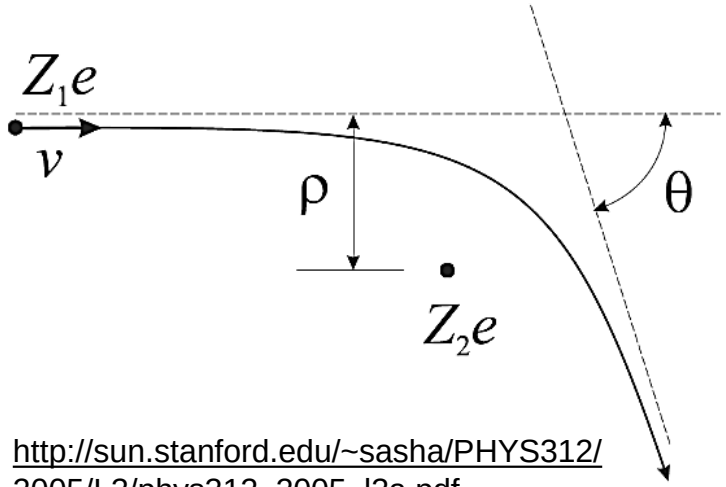

http://sun.stanford.edu/~sasha/PHYS312/2005/L3/phys312_2005_l3a.pdf

Electron effective resistivity in collisionless magnetic reconnection

$$\eta_{eff} = \frac{m_e}{e^2 n_e \langle \tau_e \rangle}$$

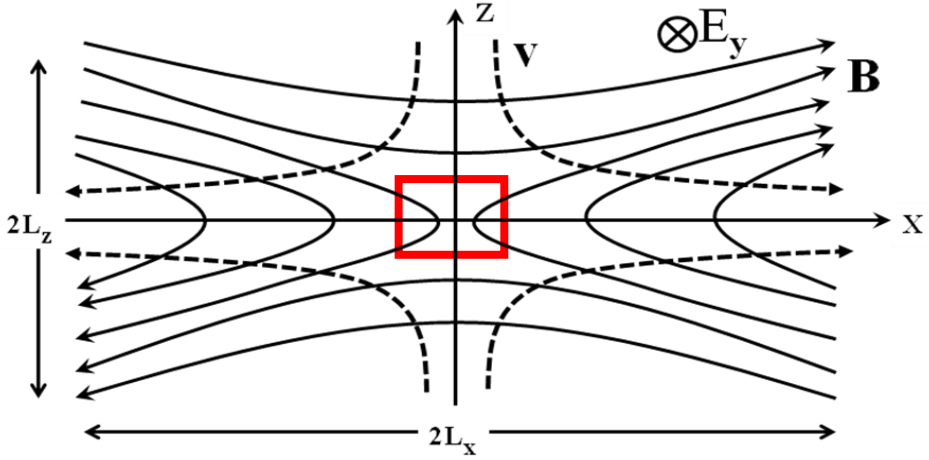

Z. W. Ma et al. Sci. Rep. 8 10521 (2018)

Physical Model

Classical (Spitzer) resistivity

$$\eta_{spz} = \frac{m_e \nu_{ei}}{e^2 n_e}$$

Coulomb collision

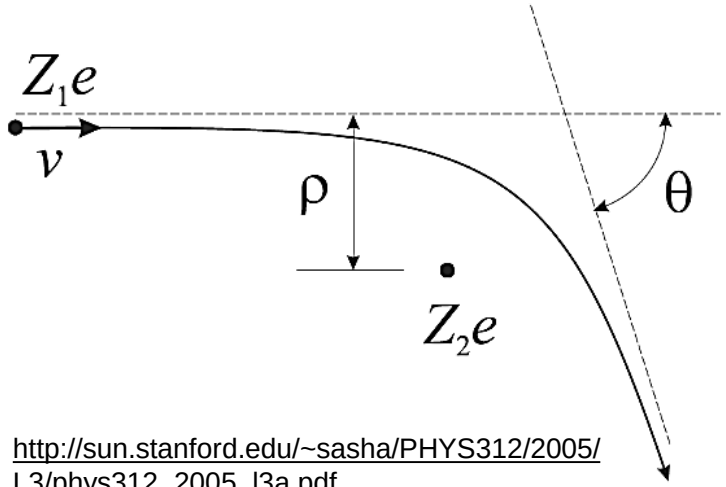

http://sun.stanford.edu/~sasha/PHYS312/2005/L3/phys312_2005_l3a.pdf

Electron effective resistivity in collisionless magnetic reconnection

$$\eta_{eff} = \frac{m_e}{e^2 n_e \langle \tau_e \rangle}$$

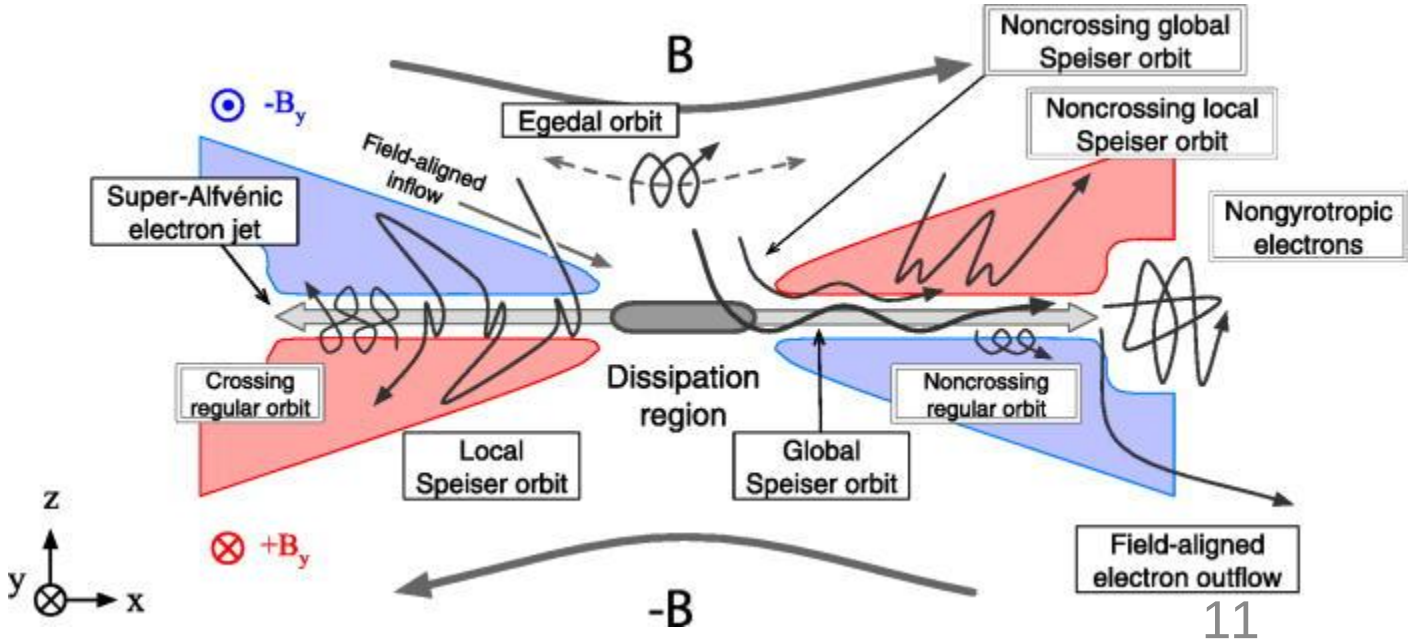

S. Zenitani et al. *Phys. Plasmas* 23, 102102 (2016)

Derivation of characteristic time

Motion equation

$$\frac{d\mathbf{v}}{dt} = \frac{q}{m}\left(\frac{\mathbf{v}\times\mathbf{B}}{c} + E_0\hat{\mathbf{y}}\right)$$

$$\mathbf{B} = B_0\frac{z\hat{\mathbf{x}}}{L_z} + B_z\frac{x\hat{\mathbf{z}}}{L_x}$$

$$\frac{d^2x}{dt^2} = \frac{J_{ey}B_z}{\rho_e L_x c}(L_{zx} + x - x_0)$$

$$\frac{d^2z}{dt^2} = \cdots$$

- L_x and L_z are characteristic scale lengths of magnetic field
- $E_{x,z} \ll E_y$ in the diffusion region
- Time scale of magnetic filed evolution $\gg$ characteristic motion time scale of particles

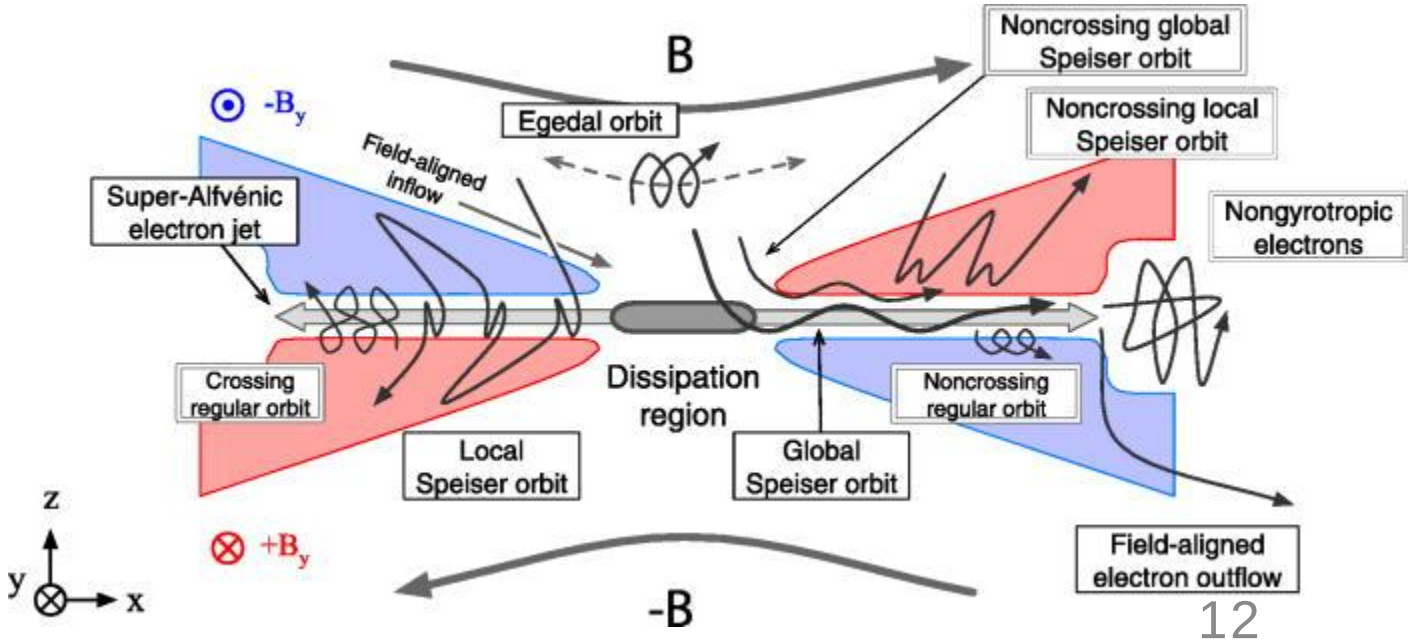

S. Zenitani et al. *Phys. Plasmas* 23, 102102 (2016)

Derivation of characteristic time

Motion equation

$$\frac{d\mathbf{v}}{dt} = \frac{q}{m}\left(\frac{\mathbf{v}\times\mathbf{B}}{c} + E_0\hat{\boldsymbol{y}}\right)$$

$$\mathbf{B} = B_0\frac{z\hat{\mathbf{x}}}{L_z} + B_z\frac{x\hat{\mathbf{z}}}{L_x}$$

- L_x and L_z are characteristic scale lengths of magnetic field
- $E_{x,z} \ll E_y$ in the diffusion region
- Time scale of magnetic filed evolution ≫ characteristic motion time scale of particles

$$\frac{d^2x}{dt^2} = \frac{J_{ey}B_z}{\rho_e L_x c}(L_{zx} + x - x_0)$$

$$\frac{d^2z}{dt^2} = \cdots$$

Speiser-like orbits

$$x(t) = x_0\cosh(t/\tau_{dx}) + v_{x0}\tau_{dx}\sinh(t/\tau_{dx})$$

Hyperbolic motion

$$z(t) = z_0\cos(t/\tau_{dz}) + v_{z0}\tau_{dz}\sin(t/\tau_{dz})$$

Oscillation motion

where

$$\tau_{dx} = \sqrt{mL_x/qv_{y0}B_z},\ \tau_{dz} = \sqrt{mL_z/qv_{y0}B_0}$$

Z. W. Ma et al. Sci. Rep. 8 10521 (2018)

Derivation of characteristic time

Since a particle could locate anywhere in the diffusion region, we solve the time $\tau(x_0)$ for a particle leaving the diffusion region from x_0, then **the averaged transit time** is

$$\tau(x_0) = \tau_{dx} \ln\left(\frac{L_0 + \sqrt{L_0^2 - x_0^2}}{x_0}\right)$$

$$\langle\tau\rangle = \frac{\int_0^{L_0} \tau(x_0) dx_0}{L_0} = \frac{\pi}{2}\tau_{dx}$$

Effective resistivity

w/o the guiding field

$$\eta_e = \frac{2}{\pi}\sqrt{\frac{m_e v_{ye} B_z}{e^3 n_e^2 L_x}}$$

w/ a guiding field

$$\eta_e = \frac{2}{\pi}\frac{\sqrt{m_e v_{ye} B_z / e^3 n_e^2 L_x}}{1 + (L_{ze}/L_{xe}) B_y \sqrt{e L_x / m_e v_{ye} B_z}}$$

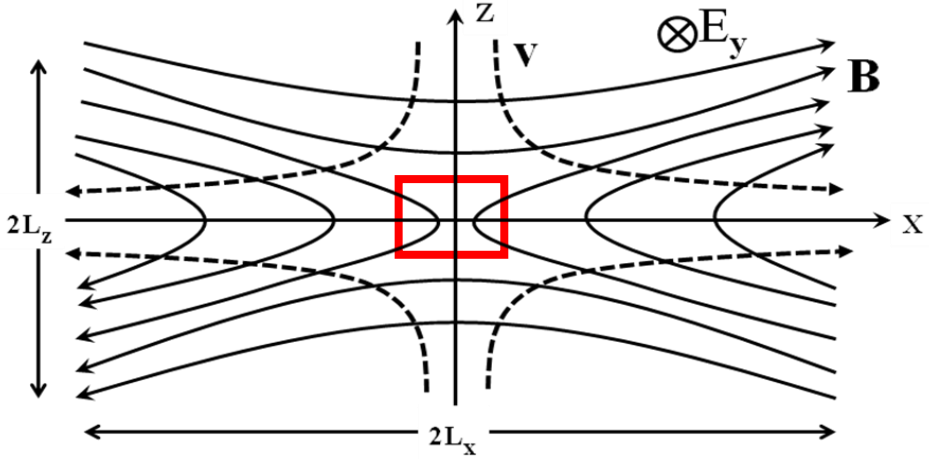

Z. W. Ma et al. Sci. Rep. 8 10521 (2018)

Outline

- Introduction
- Physical model
- Verification by PIC simulation
- Validation by in-situ satellite observation and experimental data
- Application in Hall MHD simulation
- Summary and future possible applications

Verification by PIC simulation

- Harris current sheet:

$$B_x = -B_0 \tanh(y/b),\ \rho = \rho_0 \operatorname{sech}^2(y/b) + \rho_b,$$

$$B_0 = 1.0,\ \rho_0 = 1.0,\ \rho_b = 0.2,\ b = 0.5.$$

- Simulation domain is $-12.8d_{i0} \le x \le 12.8d_{i0}$, $-6.4d_{i0} \le y \le 6.4d_{i0}$, the spatial resolution is $0.01d_{i0}$.
- The time step is $\omega_{ci}\Delta t = 0.0002$.
- 82 million ~ 1.3 billion particles for each species.
- The mass ratio m_i/m_e is varied from 25 to 400.
- The initial ion-electron temperature ratio (Tie) $T_i/T_e = 5$

PIC simulation results (benchmark)

The PIC benchmark simulation yields consistent results compared to previous simulations. The **electron off-diagonal pressure terms** balance the reconnection electric field.

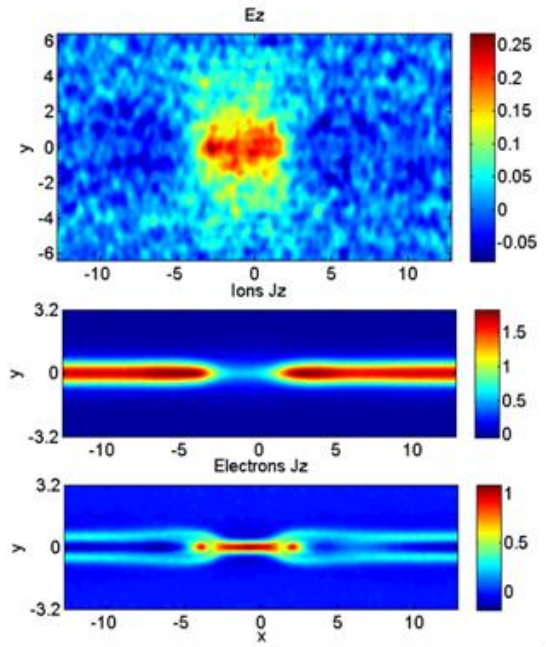

T. Chen et al. (this work)

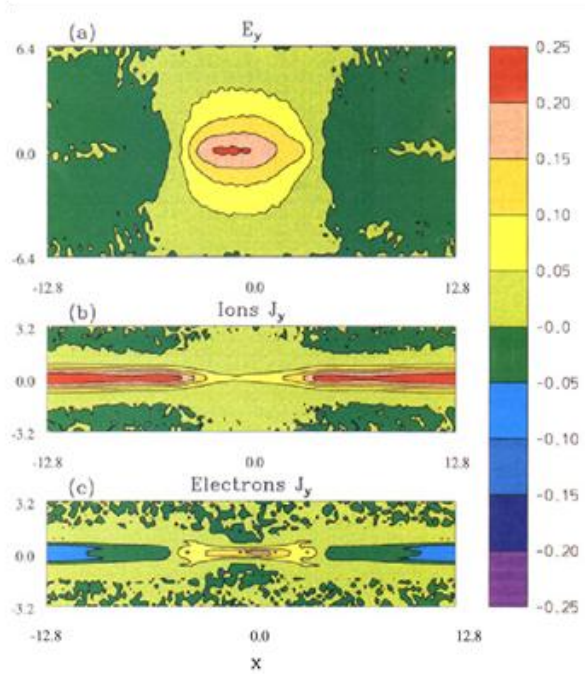

P. L. Pritchett, et al. J. Geophys. Res. 106, 4783 (2001)

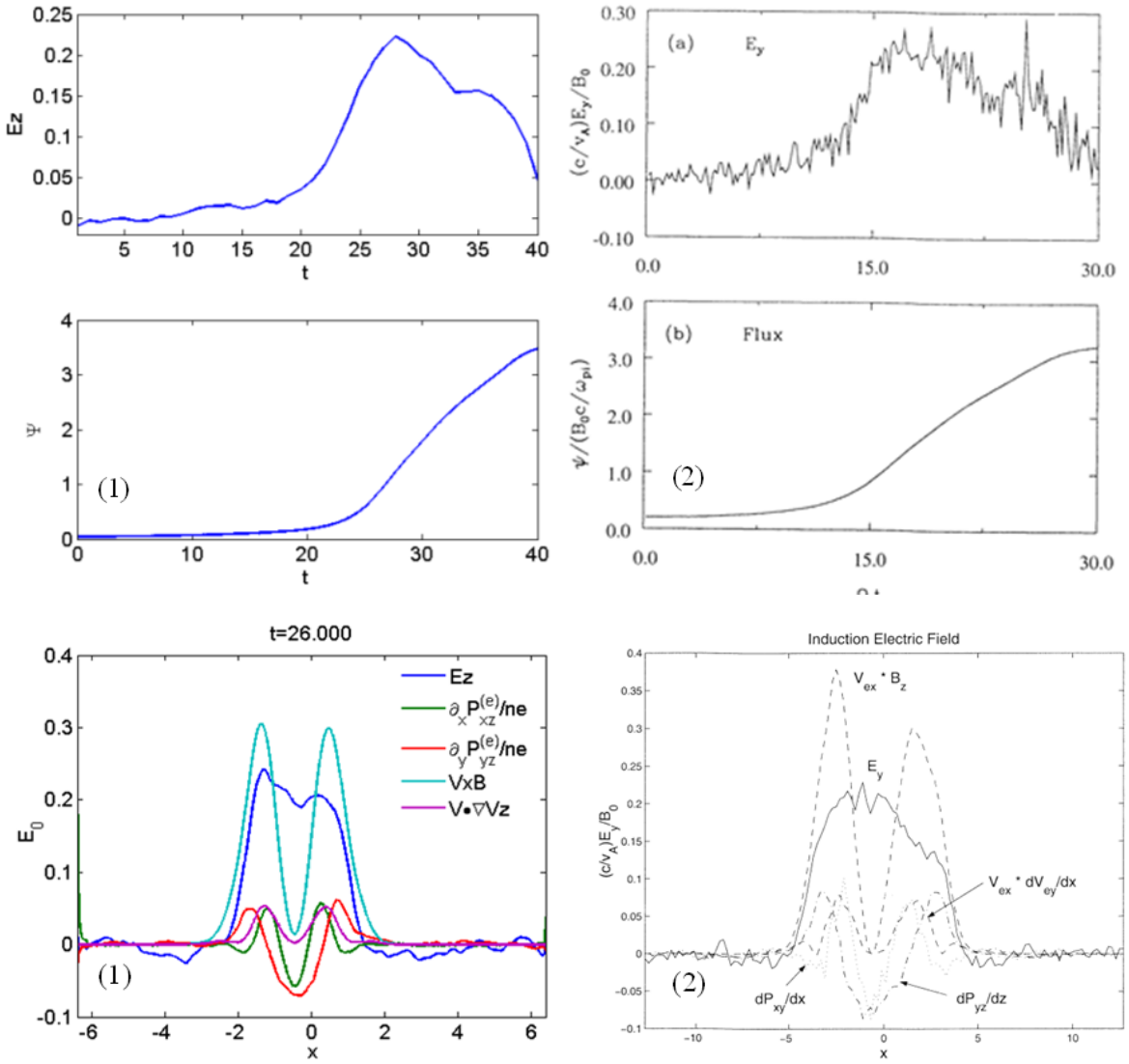

T. Chen et al. (this work)

P. L. Pritchett, et al. J. Geophys. Res. 106, 4783 (2001)

Evolutions of the effective resistivities: w/o guide field

Theoretical

Numerical

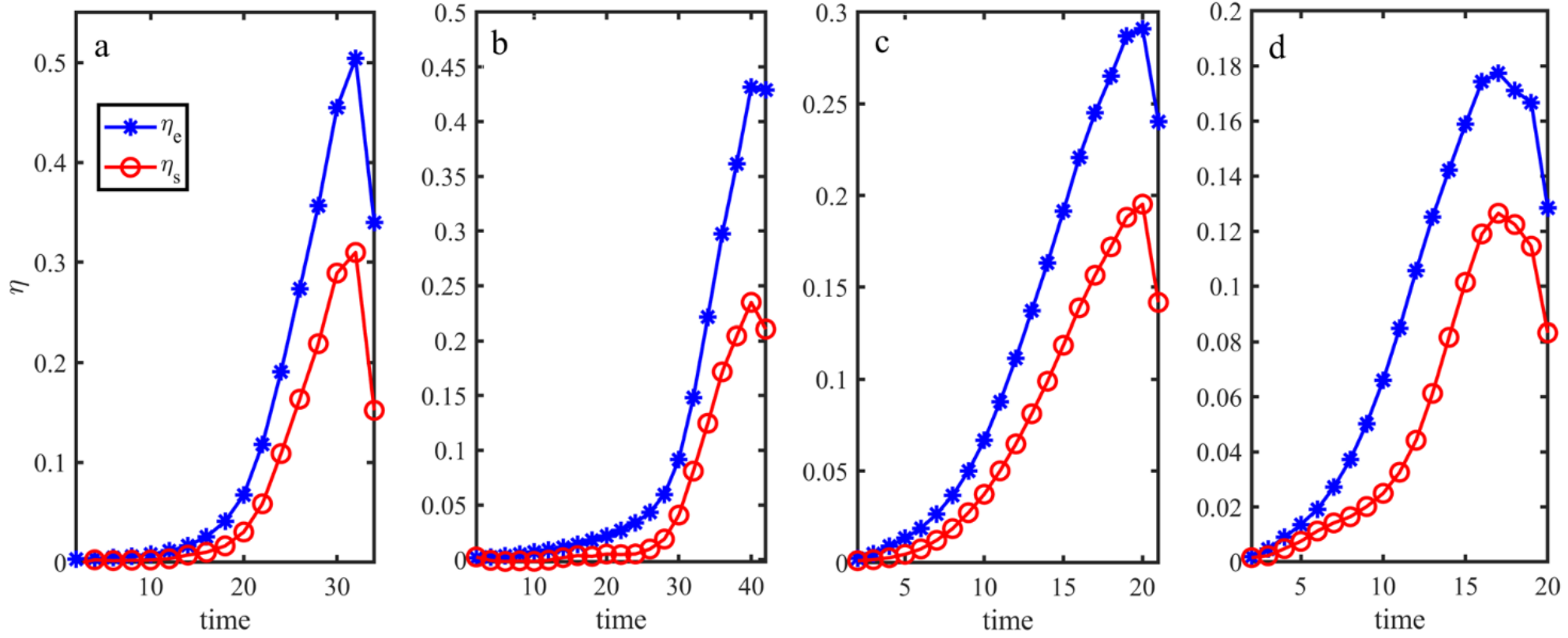

$m_i/m_e = 25$ $m_i/m_e = 100$ $m_i/m_e = 256$ $m_i/m_e = 400$

T. Chen et al. (this work)

Evolutions of the effective resistivities: w/ guide field

$m_i/m_e = 25$

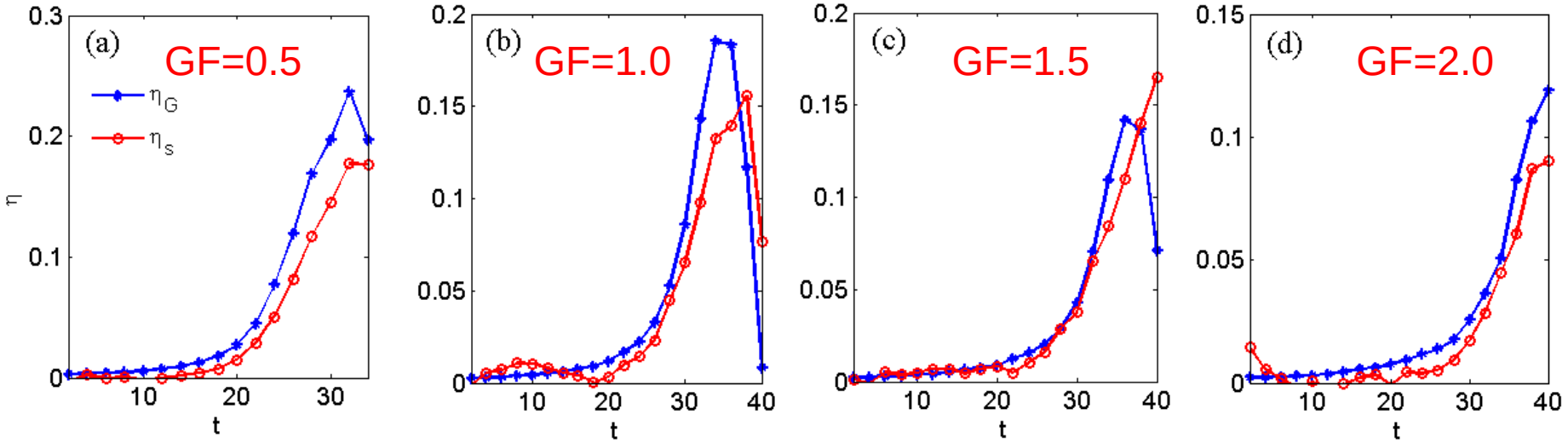

Theoretical

Numerical

GF = 1.0

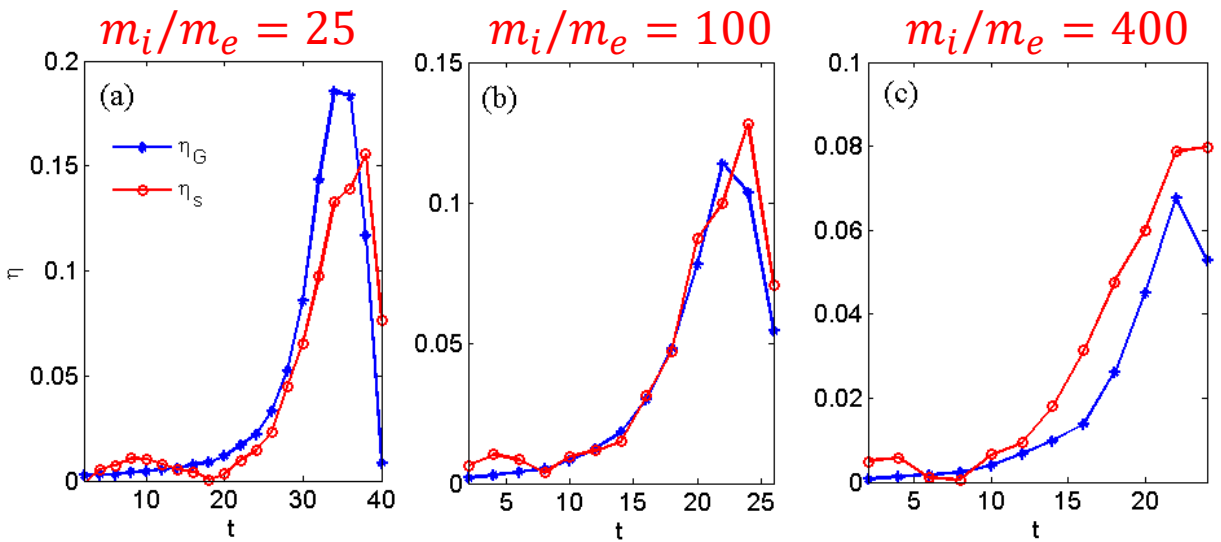

T. Chen et al. (this work)

Outline

- ❑Introduction
- ❑Physical model
- ❑Verification by PIC simulation
- ❑Validation by in-situ satellite observation and experimental data
- ❑Application in Hall MHD simulation
- ❑Summary and future possible applications

Validation by in-situ satellite observation

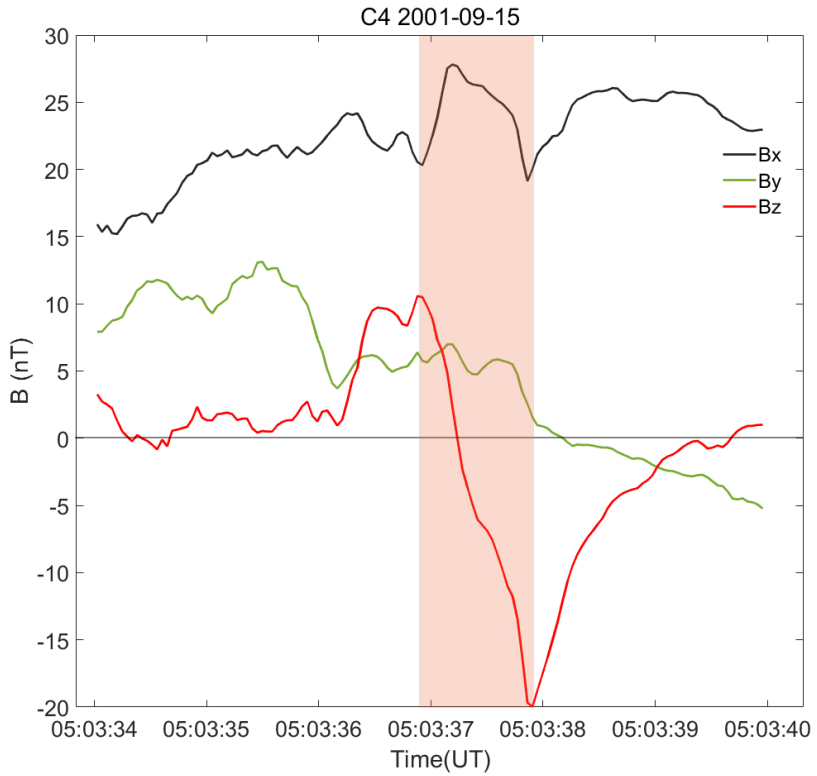

From Cluster spacecraft [**C. J. Xiao, et al. Geophys. Res. Lett. 34, L01101 (2007)**]

Another case from 10-1-2001 [**C. J. Xiao, et al. Nat. Phys. 3, 609 (2007)**]

$$\eta_{obs}/\eta_e \approx 0.8$$

From direct observation:

- $\gamma_{rec} \approx v_{in} \approx (0.07\sim0.15)v_A$
- $J \approx 2.32 \times 10^{-8} A/m^2$
- $\eta_{obs} = E_{rec}/J \approx (7.9 \sim 8.3) \times 10^4\ \Omega m$

From theoretical model:

- $n_e \approx 0.61 cm^3$
- $v_e = J/en_e \approx 168\, km/s$
- $B_z/L_x \approx 5.89 \times 10^{-11} T/m$
- $\eta_e \approx 5.0 \times 10^4 \Omega m$
- $\eta_{obs}/\eta_e \approx 1.3$

The effective resistivity from the theoretical model agrees well with that from in-situ observation!

Validation by experimental data

Resistivity enhancement as a function of collisionality for MRX:

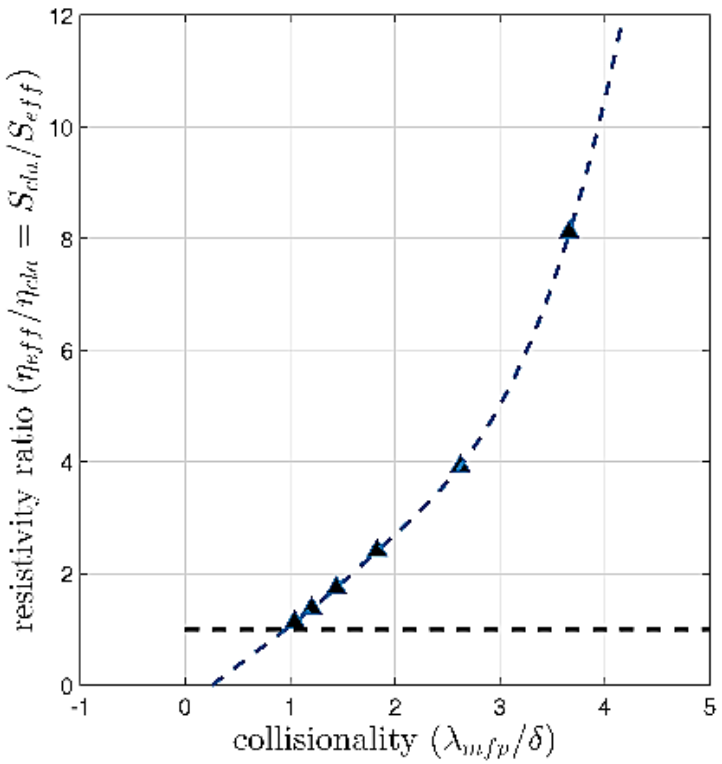

unpublished results

Estimation based on our model

$$\frac{\eta_{eff}}{\eta_{spz}} = [4\pi^{-1}\alpha^{0.5}(3\mu_0 kT_e n_e)^{-0.5}B_0]\frac{\lambda_{mfp}}{\Delta_{sp}}$$

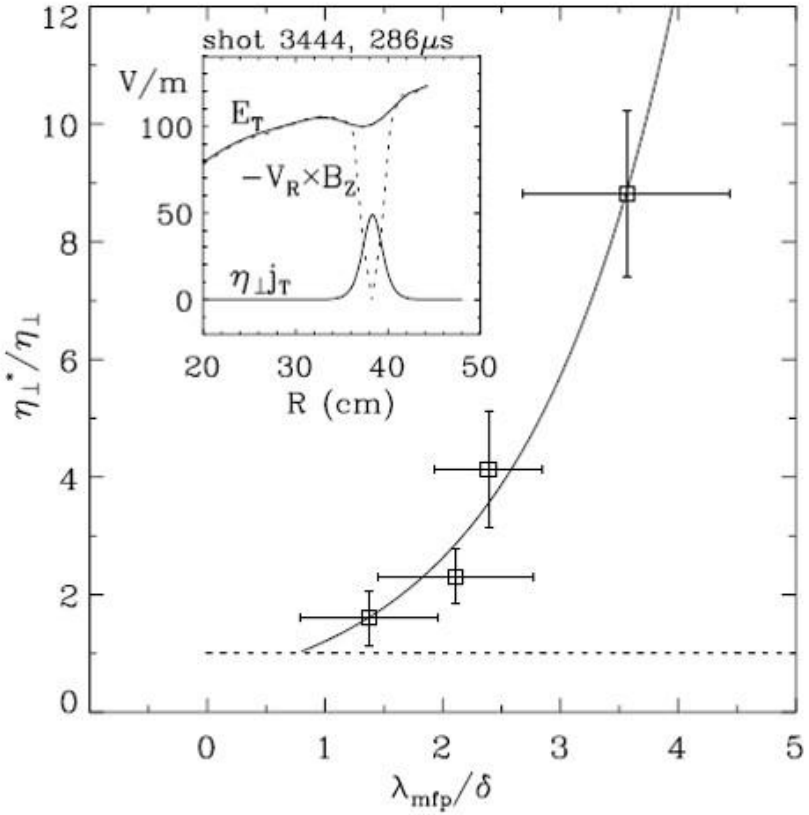

MRX experimental results from:
H. Ji, et al. Phys. Rev. Lett. 80, 3256 (1998)

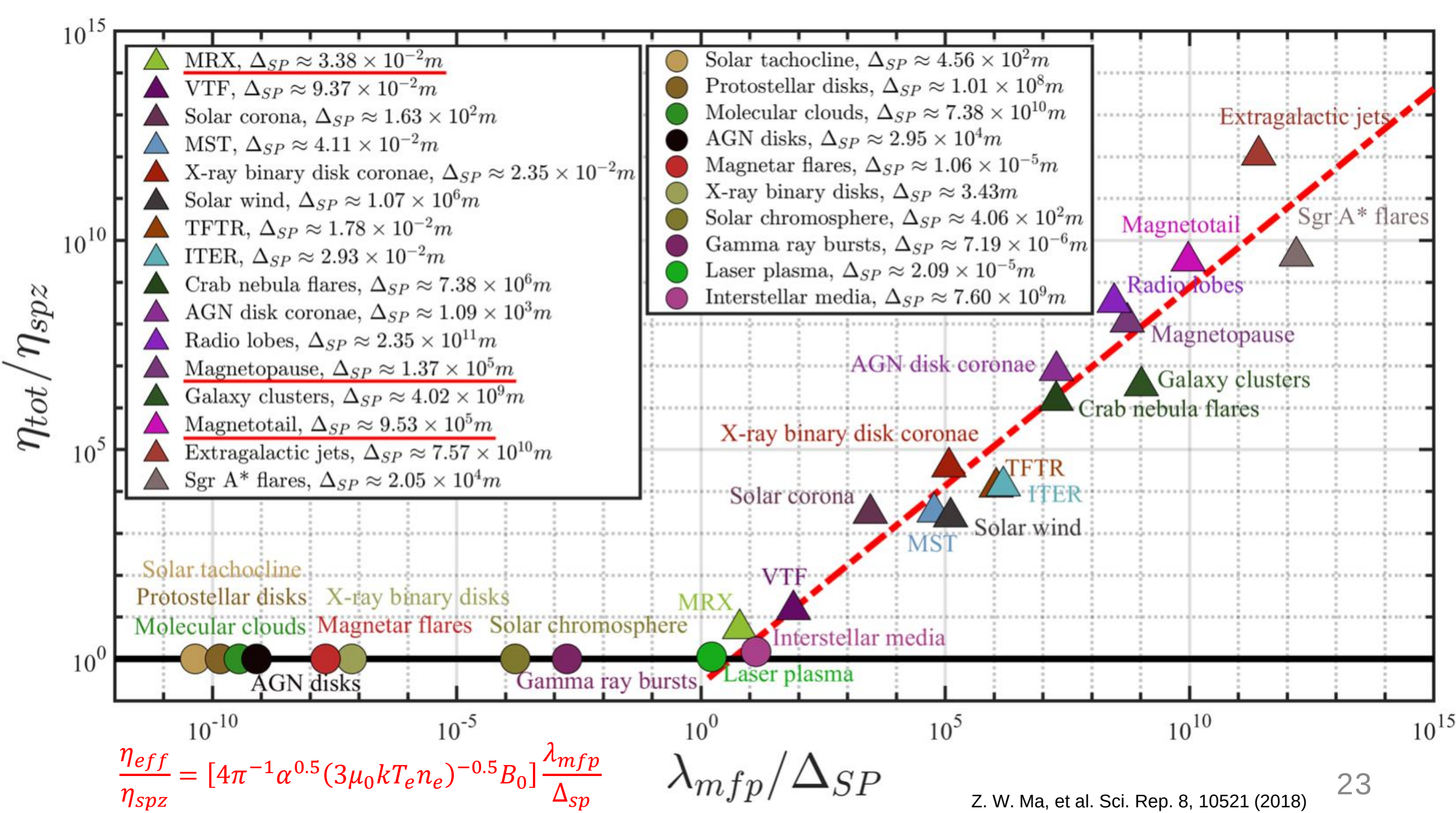

$$\frac{\eta_{eff}}{\eta_{spz}} = [4\pi^{-1}\alpha^{0.5}(3\mu_0 kT_e n_e)^{-0.5}B_0]\frac{\lambda_{mfp}}{\Delta_{sp}}$$

Z. W. Ma, et al. Sci. Rep. 8, 10521 (2018)

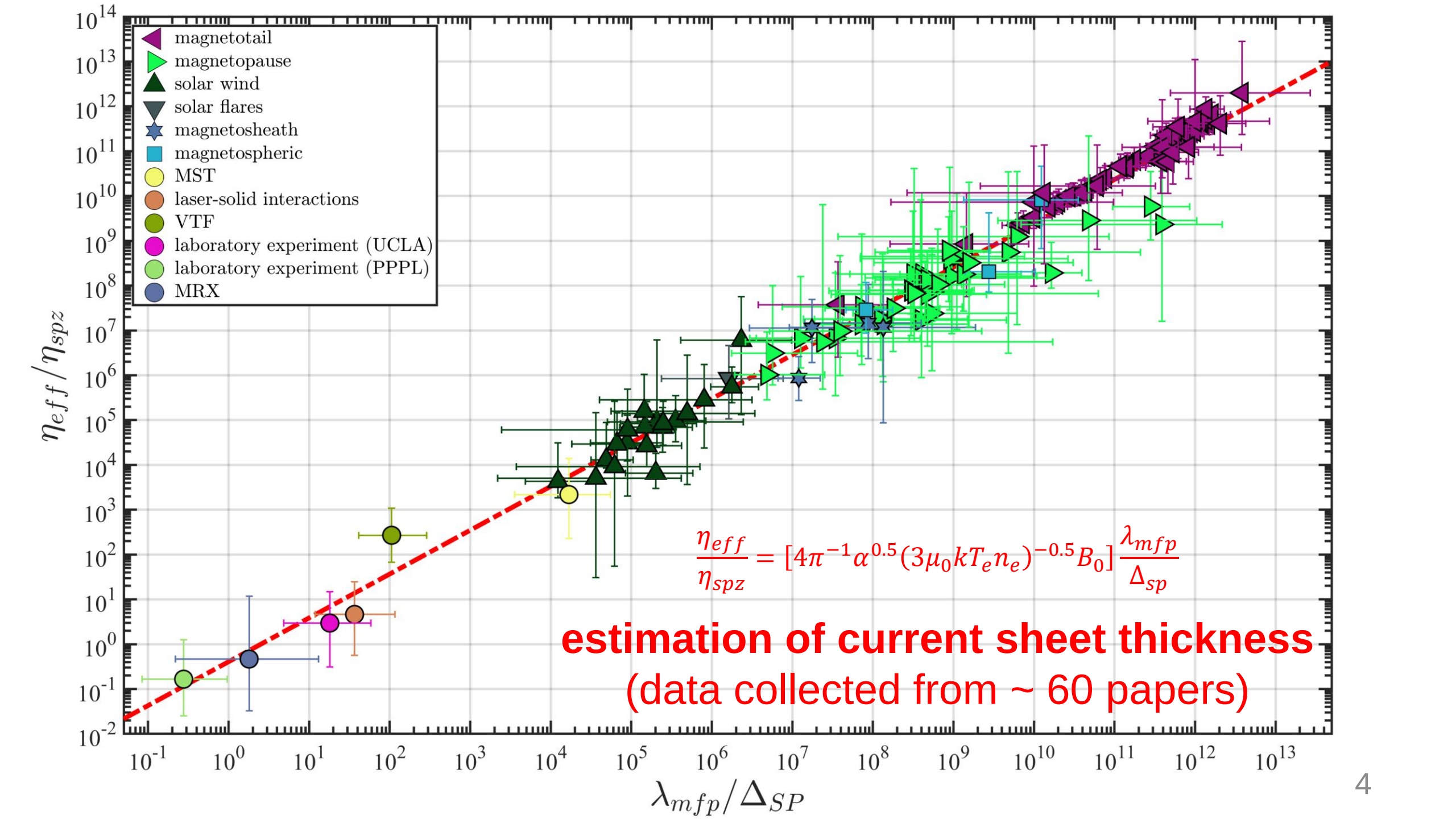
magnetotail
magnetopause
solar wind
solar flares
magnetosheath
magnetospheric
MST
laser-solid interactions
VTF
laboratory experiment (UCLA)
laboratory experiment (PPPL)
MRX
η_{eff}/η_{spz}
$\lambda_{mfp}/\Delta_{SP}$
$\frac{\eta_{eff}}{\eta_{spz}} = [4\pi^{-1}\alpha^{0.5}(3\mu_0 kT_e n_e)^{-0.5}B_0]\frac{\lambda_{mfp}}{\Delta_{sp}}$
estimation of current sheet thickness
(data collected from ~ 60 papers)

Outline

- Introduction
- Physical model
- Verification by PIC simulation
- Validation by in-situ satellite observation and experimental data
- Application in Hall MHD simulation
- Summary and future possible applications

Application in Hall MHD simulation

❑ **2.5D Hall MHD model**:

$$\frac{\partial \rho}{\partial t} = -\nabla \cdot (\rho \mathbf{v}),$$

$$\frac{\partial (\rho \mathbf{v})}{\partial t} = -\nabla \cdot [\rho \mathbf{v}\mathbf{v} + (p + B^2/2)\mathbf{I} - \mathbf{B}\mathbf{B}],$$

$$\frac{\partial \psi}{\partial t} = -\mathbf{v} \cdot \nabla \psi + \frac{1}{S_{tot}} J_y + \frac{d_i}{\rho} (\mathbf{J} \times \mathbf{B})_y,$$

$$\frac{\partial B_y}{\partial t} = -\nabla \cdot (B_y \mathbf{v}) + \mathbf{B} \cdot \nabla v_y + \frac{1}{S_{spz}} \nabla^2 B_y - d_i \nabla \left[\nabla \times \left(\frac{\mathbf{J} \times \mathbf{B} - \nabla p}{\rho} \right) \right]_y,$$

$$\frac{\partial p}{\partial t} = -\nabla \cdot (p \mathbf{v}) - (\gamma - 1) p \nabla \cdot \mathbf{v} + \frac{1}{S_{tot}} J_y^2 + \frac{1}{S_{spz}} (J_x^2 + J_z^2).$$

where $S_{tot} = \tau_{R,tot}/\tau_A$, $\tau_{R,tot} = 4\pi d_i^2/c^2 \left(\eta_{spz} + \eta_{eff}\right)$, $\eta_{spz} \simeq 0.001$

$$\eta_{eff} \approx \frac{m_e^2/e^2\rho_e}{1 + \sqrt{m_e J_{ey}/m_i J_{iy}}} \sqrt{\frac{J_{ey} B_z}{\rho_e L_{zx} c}} \exp\left[-\left(\frac{z - z_0}{\lambda_b} \right)^2 - \left(\frac{x - x_0}{x_2 - x_0} \right)^2 \right]$$

❑ **Harris current sheet** $[-12.8d_{i0} \le x \le 12.8d_{i0},\ -6.4d_{i0} \le y \le 6.4d_{i0}]$:

$$B_x = -B_0 \tanh(y/b),\ \rho = \rho_0 \operatorname{sech}^2(y/b) + \rho_b,$$

$$B_0 = 1.0,\ \rho_0 = 1.0,\ \rho_b = 0.2,\ b = 0.5.$$

H. W. Zhang, et al. J. Geophys. Res. Space Phys. 130, e2025JA034289 (2025)

Application in MHD simulation (without Hall effect, $d_i = 0$)

- With the effective resistivity, the peak **reconnection rate** ($\sim \mathbf{0.1}\boldsymbol{B_0 v_A}$) is increased by more than an order of magnitude compared with the η_{spz} MHD case ($\sim 0.01 B_0 v_A$).

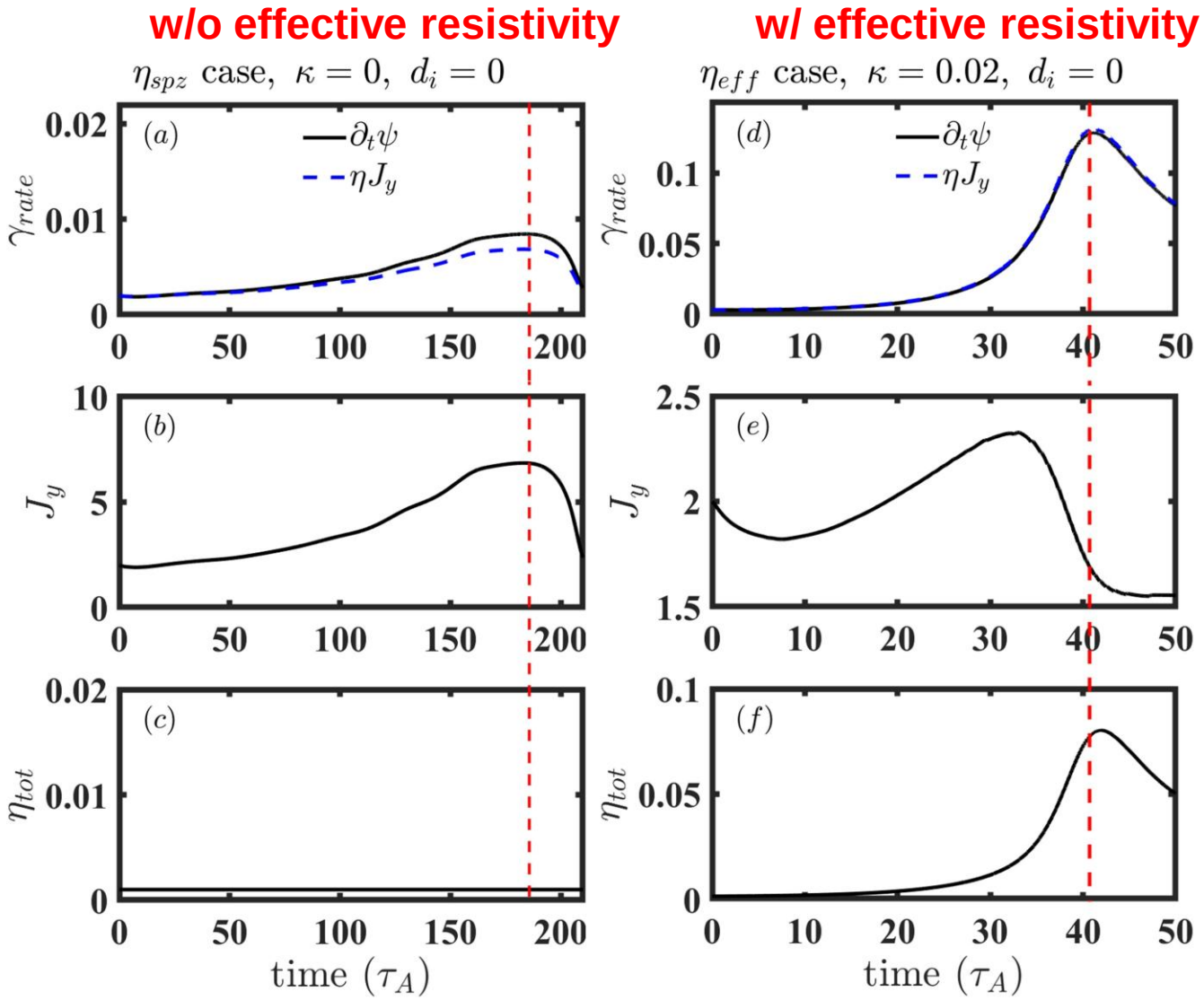

H. W. Zhang, et al. J. Geophys. Res. Space Phys. 130, e2025JA034289 (2025)

Application in MHD simulation (without Hall effect, $d_i = 0$)

- With the effective resistivity, the peak **reconnection rate** ($\sim \mathbf{0.1}\boldsymbol{B_0 v_A}$) is increased by more than an order of magnitude compared with the η_{spz} MHD case ($\sim 0.01 B_0 v_A$).
- **The current sheet width is wider**, because the resistive dissipation region increases significantly after applying the effective resistivity, as predicted by the Sweet-Parker model $\left(\lambda_b \approx L S_L^{-1/2}\right)$.

w/o effective resistivity

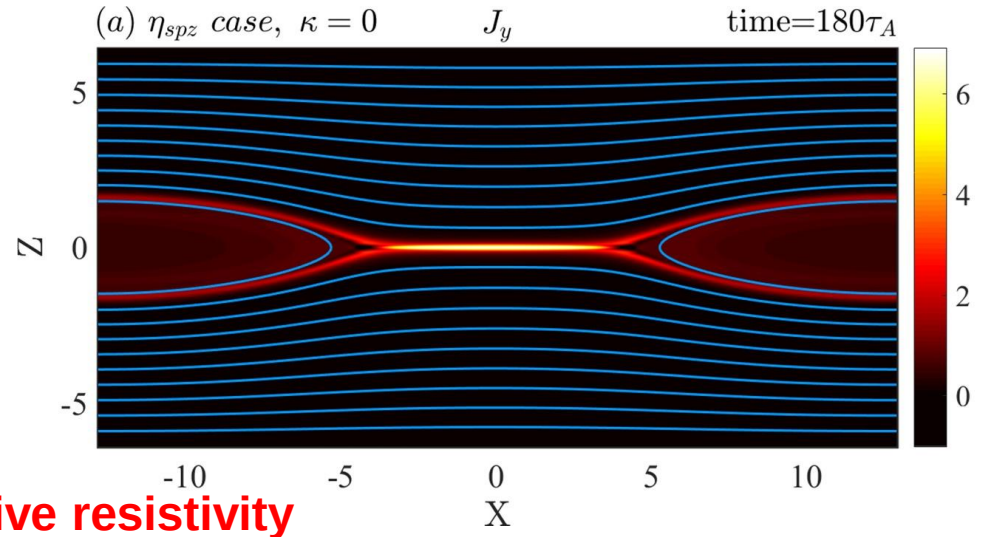

w/ effective resistivity

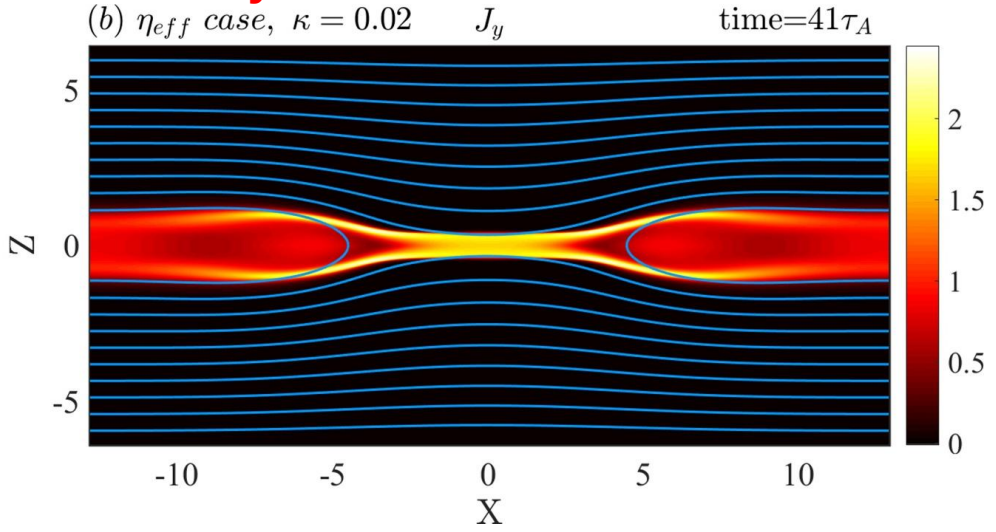

H. W. Zhang, et al. J. Geophys. Res. Space Phys. 130, e2025JA034289 (2025)

Application in Hall MHD simulation (with Hall effect, $d_i = 1$)

- With the effective resistivity, the peak **reconnection rate is** $\sim \mathbf{0.25} B_0 v_A$.

Hall MHD w/o effective resistivity

Hall MHD w/ effective resistivity

PIC simulation

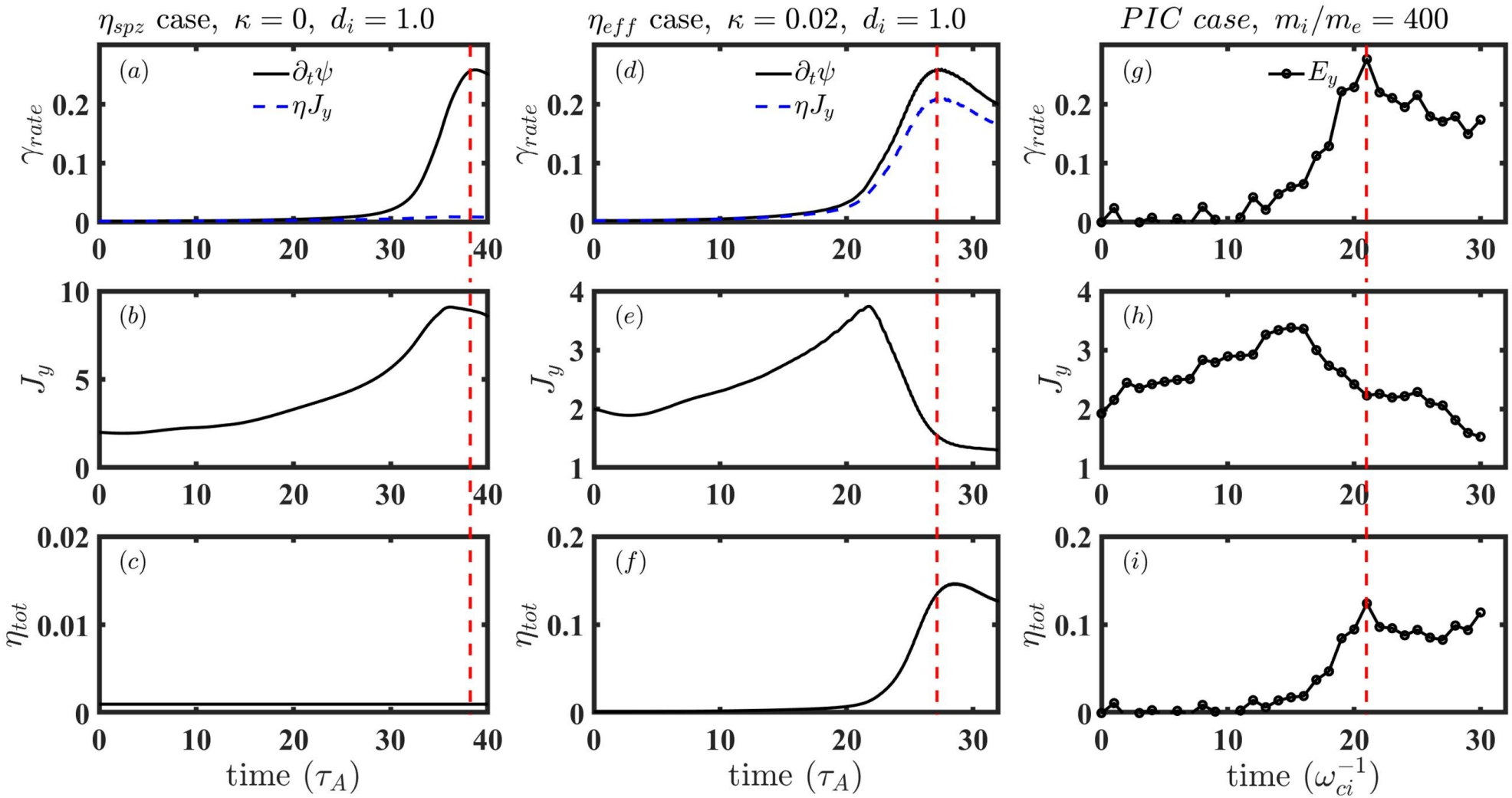

H. W. Zhang, et al. J. Geophys. Res. Space Phys. 130, e2025JA034289 (2025)

Application in Hall MHD simulation (with Hall effect, $d_i = 1$)

- With the effective resistivity, the peak **reconnection rate is** $\sim \mathbf{0.25} B_0 v_A$.
- No singularity in current density at the X-point.
- Consistent with PIC simulation results.

- Application in cases with guiding field has been successfully implemented and will be presented in future publication.

Hall MHD w/o effective resistivity

Hall MHD w/ effective resistivity (<< 100 core-hours)

PIC simulation (~100k core-hours for 400 ppc)

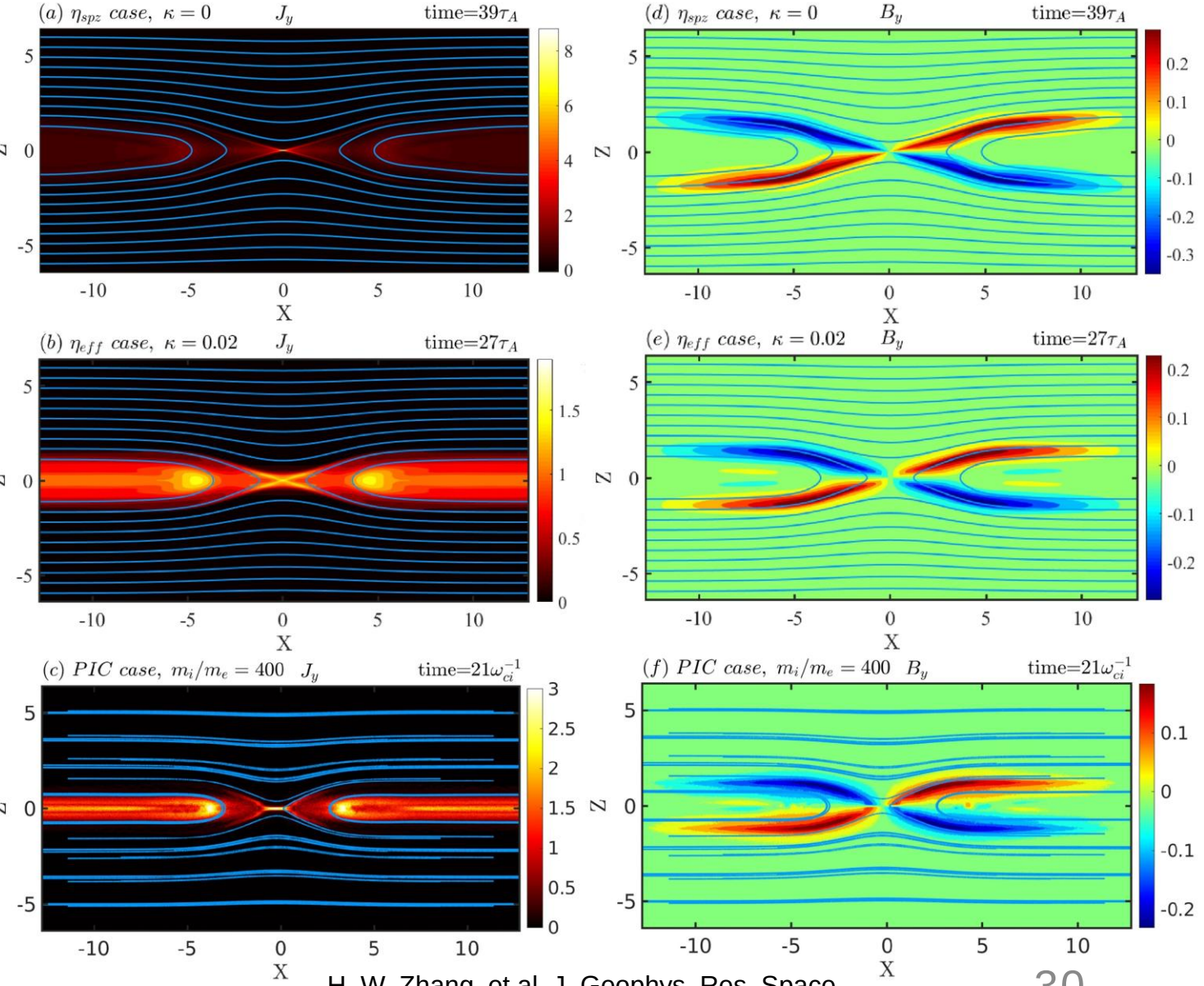

H. W. Zhang, et al. J. Geophys. Res. Space Phys. 130, e2025JA034289 (2025)

Outline

- Introduction
- Physical model
- Verification by PIC simulation
- Validation by in-situ satellite observation and experimental data
- Application in Hall MHD simulation
- Summary and future possible applications

Summary

- A physical model of **effective resistivity** for **fast collisionless reconnection** is proposed based on the characteristic motion of electrons in the diffusion region.
- Effective resistivity from our model is in **good agreement** with that measured from **PIC simulation**, and is **validated by in-situ satellite and experimental observations**.
- Using the model, we can explain the **characteristic scales of current sheet** in space and laboratory plasmas.
- Reconnection dynamics in Hall MHD with inclusion of the effective resistivity are **quantitatively consistent with those in PIC**.
- The effective resistivity significantly increases the reconnection rate in MHD simulations to a reasonable value of $\sim \mathbf{0.1} B_0 v_A$ **(w/o Hall) and** $\sim \mathbf{0.25} B_0 v_A$ **(w/ Hall)**.
- The more general effective resistivity model **incorporating the guiding field and field asymmetry** has been developed and validated, and will be implemented in future MHD simulations.

Thanks for your attention!

- Z. W. Ma, et al. Sci. Rep. 8, 10521 (2018)
- H. W. Zhang, et al. J. Geophys. Res. Space Phys. 130, e2025JA034289 (2025)

Future possible applications

- ❑ Automated X-line tracking technology + effective resistivity model (with guide field).
- ❑ Applications in 3D magnetized plasma systems: **space weather simulator**, resistive MHD simulations of **astrophysics**, collisionless **tearing mode** in magnetic confined **fusion devices**.

Corona, solar wind, magnetotail

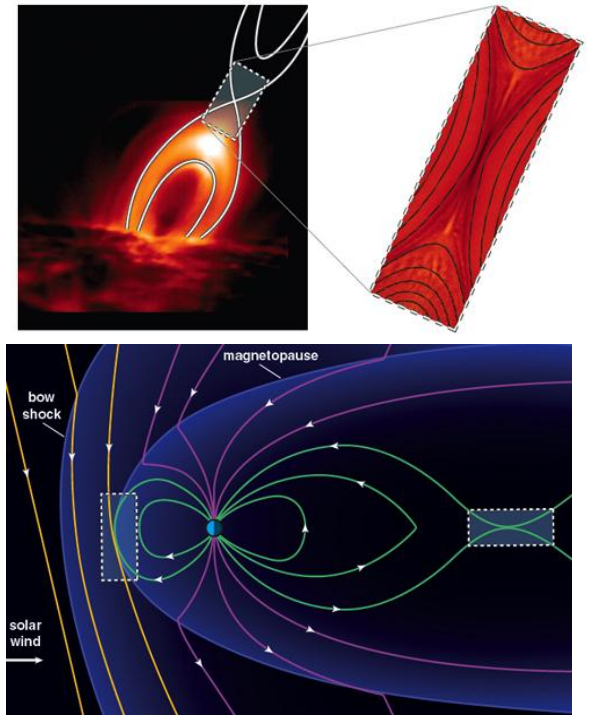

J. L. Burch and J. F. Drake, 2009

Resistive MHD simulation of black hole accretion disks

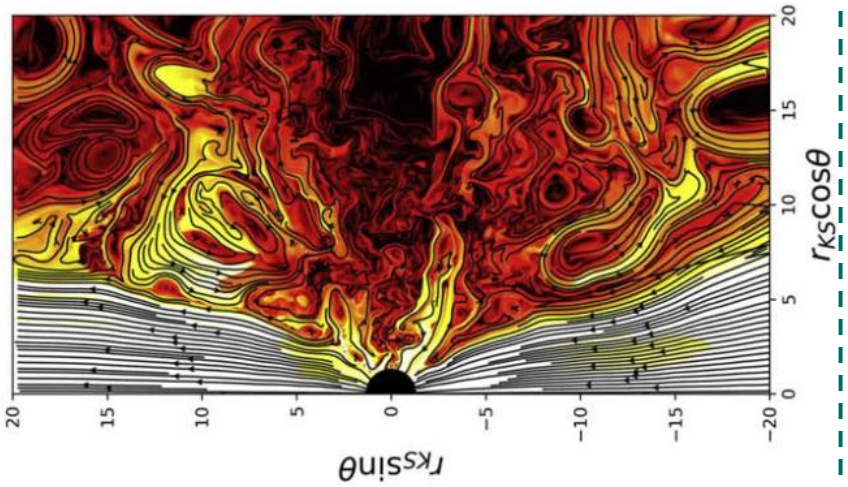

B. Ripperda, et al. Astrophys. J. 900, 100 (2020)

Poincaré-Hopf index: mapping X/O-points of sawtooth/tearing mode in tokamak

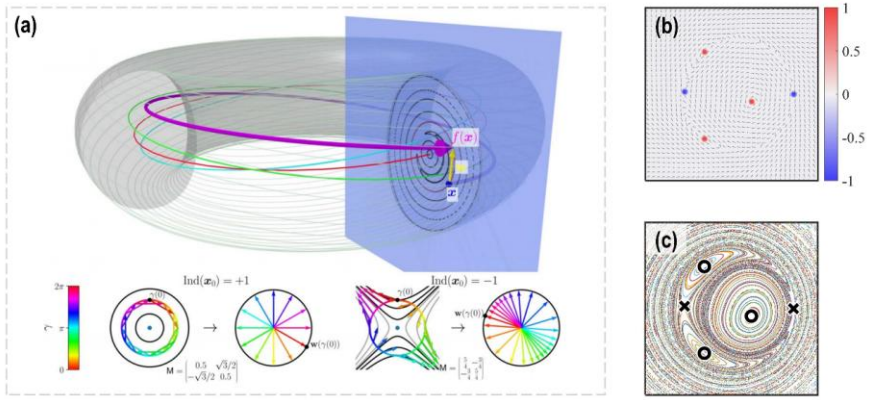

C. B. Smiet, et al. Plasma Phys. Control. Fusion 62, 025007 (2020)
H. X. Zhang, et al. Nucl. Fusion 66, 032001 (2026)

Back up slides

Previous explanation for reconnection electric field: the electron off-diagonal pressure term

PIC simulation

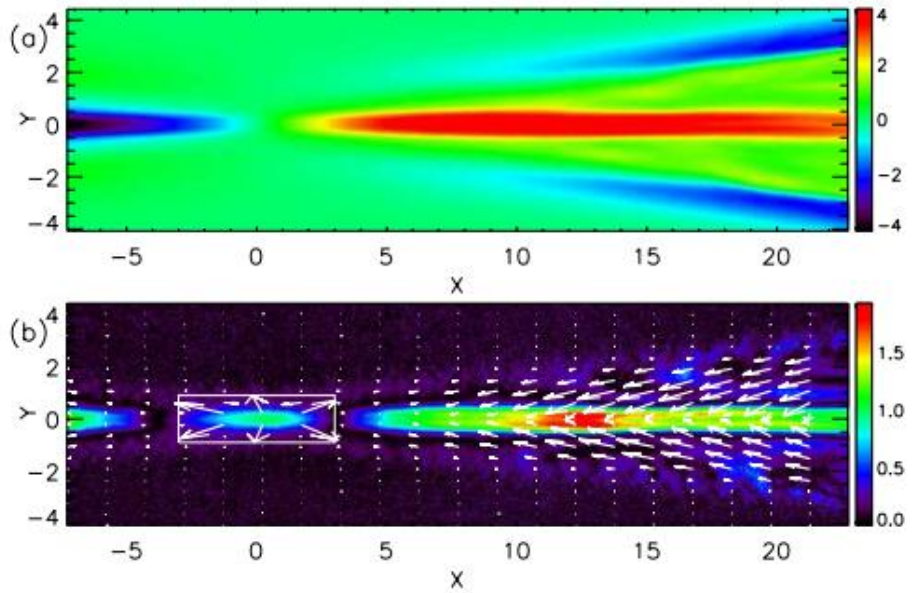

FIG. 3 (color online). Blowups around the x line (averaged from $t = 172.5$ to 174.5) for the run in Fig. 2(a). In (a) The electron outflow velocity v_{ex}. In (b) Momentum flux vectors, $\mathbf{\Gamma} = p_{exz}\hat{\mathbf{x}} + p_{eyz}\hat{\mathbf{y}}$ (vectors in box surrounding x line are multiplied by 20), with a background color plot of $|[E_z + (\mathbf{v}_e \times \mathbf{B}/c)_z]/E_z|$.

M. A. Shay, et al. Phys. Rev. Lett. 99, 155002 (2007)

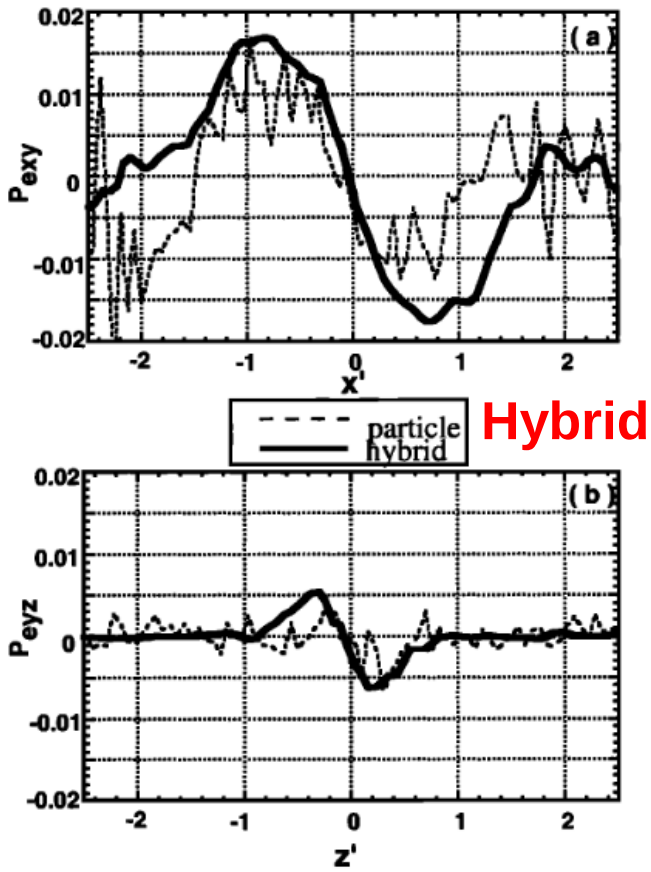

Hybrid simulation

Figure 4. (a) Comparison along the $x' = x - x_0$ axis of P_{xy} component of the electron pressure tensor at $t = 17$ for particle (dashed curves) and hybrid (solid curves) simulations; (b) Comparison along the z axis of P_{yz} component of the electron pressure tensor at $t = 17$ for particle (dashed curves) and hybrid (solid curves) simulations. The plots are centered around the dominating X points.

M. M. Kuznetsova, et al. J. Geophys. Res. 106, 3799 (2001)

Derivation of characteristic time

Lorentz force

$$\frac{d\mathbf{v}}{dt} = \frac{q}{m}\left(\frac{\mathbf{v}\times\mathbf{B}}{c} + E_0\hat{\boldsymbol{y}}\right)$$

$$\mathbf{B} = B_0\frac{z\hat{\mathbf{x}}}{L_z} + B_z\frac{x\hat{\mathbf{z}}}{L_x}$$

- L_x and L_z are characteristic scale lengths of magnetic field
- $E_{x,z} \ll E_y$ in the diffusion region
- Time scale of magnetic filed evolution ≫ characteristic motion time scale of particles

The percentage for particles with $\delta v_y/v_{y0} > 0.2$ is 9%.

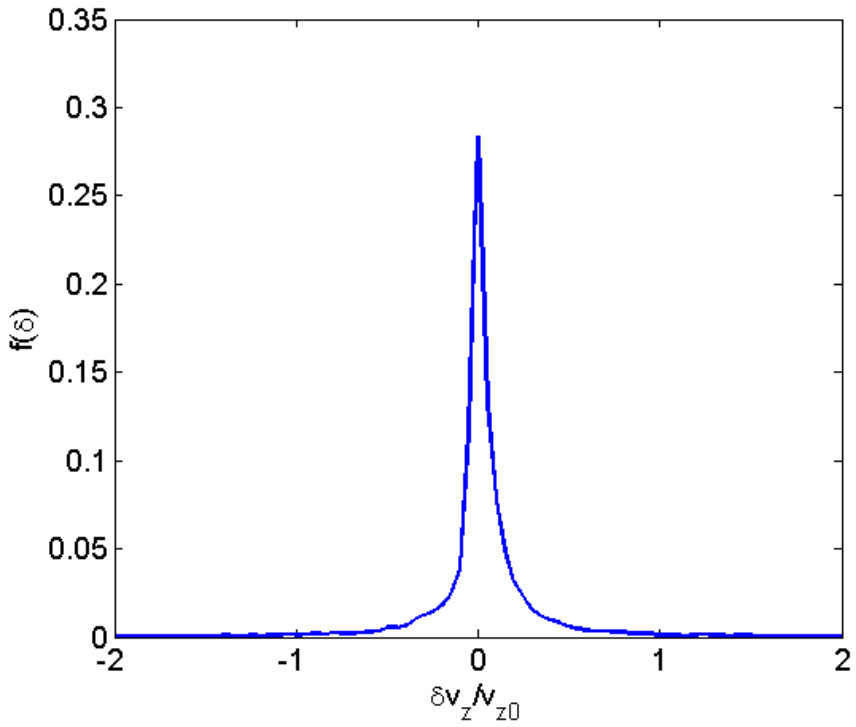

The distribution of velocity change in the *y* direction within one Alfvenic time.

Z. W. Ma et al. Sci. Rep. 8 10521 (2018)

Validation by experimental data

Estimation of Sweet-Parker current sheet thickness

$$\eta^{spz} = \frac{m_e \nu_{e,i}}{n_e e^2} \qquad \lambda_{mfp} = \frac{\langle v_{the} \rangle}{\nu_{e,i}}$$

$$\frac{\partial B_z}{\partial x} \approx \alpha \cdot \frac{\partial B_x}{\partial z}, \qquad \eta_{eff} = \frac{m_e}{e^2 n_e \langle \tau_e \rangle}$$

$$\frac{\eta_{eff}}{\eta_{spz}} = [4\pi^{-1}\alpha^{0.5}(3\mu_0 k T_e n_e)^{-0.5} B_0] \frac{\lambda_{mfp}}{\Delta_{sp}}$$

where

$$\Delta_{sp} \approx L \cdot S_{sp}^{-1/2}$$

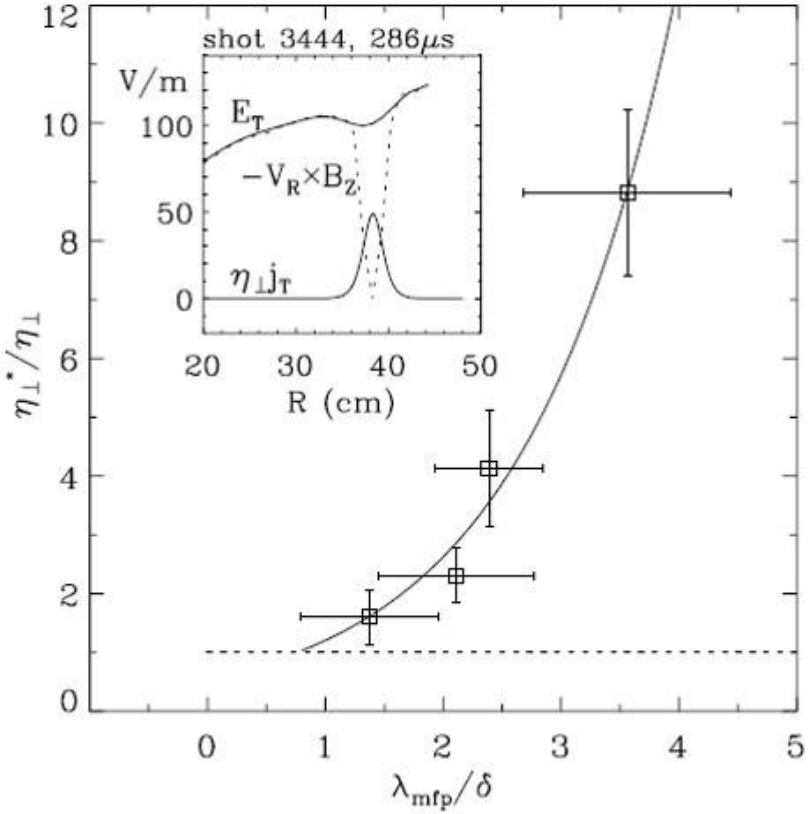

MRX experimental results from:
H. Ji, et al. Phys. Rev. Lett. 80, 3256 (1998)